Drug Design, Development and Therapy

Dovepress
open access to scientific and medical research

Open Access Full Text Article

ORIGINAL RESEARCH

Andrographolide Inhibits Static Mechanical Pressure-Induced Intervertebral Disc Degeneration via the MAPK/Nrf2/HO-1 Pathway

Cunxin Zhang[1,2], Ziang Lu[3], Chaoliang Lyu[2], Shanshan Zhang[4], Dechun Wang[1]

[1]Department of Spine Surgery, Qingdao Municipal Hospital, Shandong University, Qingdao, 266061, People's Republic of China; [2]Department of Spine Surgery, Jining No.1 People's Hospital, Jining, 272011, People's Republic of China; [3]Jining Medical University, Jining, 272067, People's Republic of China; [4]Department of Neurology, Jining No.1 People's Hospital, Jining, 272011, People's Republic of China

Correspondence: Dechun Wang, Department of Spine surgery, Qingdao Municipal Hospital, Shandong University, 5# Donghai Road, Shinan District, Qingdao, 266061, People's Republic of China, Tel +86+18661809296, Fax +86-0532-82716868, Email dechun-w@163.com

Purpose: To explore the molecular mechanism by which andrographolide (ADR) inhibits static mechanical pressure-induced apoptosis in nucleus pulposus cells (NPCs) and to assess the role of ADR in inhibiting IDD.

Methods: Hematoxylin-eosin (HE), toluidine blue, and immunofluorescence staining were used to identify NPCs. An NPC apoptosis model was constructed using a homemade cell pressurization device. The proliferation activity, reactive oxygen species (ROS) content, and apoptosis rate were detected using kits. The expression of related proteins was detected using Western blot. A rat tailbone IDD model was constructed using a homemade tailbone stress device. HE staining and safranine O-fast green FCF cartilage staining were used to observe the degeneration degree of the intervertebral disk.

Results: ADR inhibits static mechanical pressure-induced apoptosis and ROS accumulation in NPCs and improves cell viability. ADR can promote the expression of Heme oxygenase-1 (HO-1), p-Nrf2, p-p38, p-Erk1/2, p-JNK, and other proteins, and its effects can be blocked by inhibitors of the above proteins.

Conclusion: ADR can inhibit IDD by activating the MAPK/Nrf2/HO-1 signaling pathway and suppressing static mechanical pressure-induced ROS accumulation in the NPCs.

Keywords: andrographolide, intervertebral disc degeneration, nucleus pulposus cells, apoptosis, reactive oxygen species, HO-1

Introduction

Low back pain (LBP) is a major health and social problem and the leading cause of disability in most older adults. Studies have shown that approximately 80% of adults will experience LPB at some point in their lives.[1] Although LBP has little impact on mortality, it is associated with considerable medical and non-medical related costs to patients, their families, and healthcare institutions.[2] As societies age globally, these costs are likely to continue to rise, imposing further pressure on healthcare delivery, particularly in poor and developing countries.[3] The load-bearing structures that make up the lumbar spine (eg, intervertebral disk [IVD], articular tuberosity, anterior and posterior longitudinal ligaments, spinous process, interspinous ligaments, and paravertebral muscles) are susceptible to different mechanical stresses. Stress injury to each of these structures, individually or in combination, can lead to LBP, and mechanical stress-induced IDD is a major factor in LBP.[4] Previous studies have shown that although numerous factors contribute to IDD, such as mechanical loading, genetic factors, nutritional deficiencies, occupational exposure, lack of exercise, alcohol and tobacco consumption, and aging,[5] an increasing number of studies have reported the important effect of mechanical stress on IDD.[6] Therefore, studying the molecular mechanism of IDD caused by mechanical stress and identifying corresponding therapeutic targets is a current research hot spot for LBP; success in this area will provide a new theoretical basis and therapeutic methods for the clinical treatment of LBP and has important practical significance.

Received: 12 October 2022
Accepted: 10 February 2023
Published: 20 February 2023

As a load-bearing and cushioning unit of the spine, the main function of the IVD is to maintain normal spine height and physiological curvature, and disperse and evenly transfer mechanical stress.[7] Rotation, bending, weight bearing, and stretching activities of the spine induce various deformations in the IVD, which causes the nucleus pulposus (NP) to be in a constant state of high pressure and deformation. Even when the IVD is not under any pressure, the pressure inside the IVD is not zero.[8] From birth, changes in mechanical stress affect the function and behavior of IVD cells, including their differentiation, metabolism, proliferation, and survival.[9]

Under the influence of mechanical stress and other factors, notochordal cells gradually disappear from the IVD and transform into nucleus pulposus cells (NPCs), which have the ability to produce and maintain the extracellular matrix (ECM). Although certain mechanical stresses can promote NPC division and proliferation, excessive mechanical stress can also inhibit NPC proliferation and even induce apoptosis.[10] Eventually, this leads to fibrosis of the nucleus pulposus tissue, which changes from a translucent gel to stronger cartilage tissue, coupled with loss of normal function.

The main role of NPCs is to generate and maintain ECM, and the progression of IDD is initiated and accelerated by NPC depletion and ECM degradation.[11] Although many factors contribute to NPC apoptosis, the effect of external undue mechanical stress is the main factor.[12] Indeed, AS mechanical stress can increase reactive oxygen species (ROS) production to induce NPC apoptosis, inhibition of ROS production may be an important target to inhibit mechanical stress-induced IDD.

Andrographolide (ADR) is a diterpenoid containing a γ-lactone ring that is isolated from the herb *Andrographis paniculata*. Clinical studies have shown that ADR has antioxidant, anti-inflammatory, and anti-cancer bioactivities and can be used to treat various diseases, including osteoarthritis,[13] upper respiratory disease, epidermal chloasma,[14] hyperlipidemia,[15] hand, foot, and mouth disease,[16] and multiple sclerosis.[17] However, researchers are most interested in the powerful antioxidant activity of ADR. ADR acts directly by neutralizing free radicals and indirectly by protecting mitochondrial integrity, inhibiting pro-oxidant enzymes, and/or activating antioxidant enzymes.

Whether ADR can inhibit IDD by suppressing mechanical pressure-induced ROS accumulation has not yet been reported. In this study, we creatively link ADR with mechanical pressure degeneration of IVD, with the aim to explore the role and molecular mechanism of ADR in static mechanical pressure-induced IDD, and provide a theoretical basis and new targets for the prevention and treatment of IDD.

Materials and Methods

Ethics Statement

All the animal procedures were performed in accordance with the Guidelines for Care and Use of Laboratory Animals of the National Institutes of Health. All animal experiments were approved by the Institutional Review Board (or Ethics Committee) of Jining No.1 People's Hospital (JNRM-2022-DW-023).

Cell Culture

Four eight-week-old Sprague–Dawley (SD) rats were euthanized using the cervical dislocation method and the NP tissues of the thoracic and lumbar spine were obtained aseptically. Trypsin 0.25% (Upsilon, Beijing, China) was added and the supernatant was removed via centrifugation after digestion at 37°C for 20 min. Subsequently, 0.2% type II collagenase (Solarbio, Beijing, China) was added and digested for 1 h at 37°C, and the supernatant was removed via centrifugation. Subsequently, DMEM/F12 medium (Gibco, Grand Island, NY, USA) (containing 10% FBS, 1% penicillin-streptomycin) was added to resuspend the cell pellet. The cell density was adjusted to 3–5 × 10^5/mL and inoculated into 25 cm^2 cell culture flasks, before placing in an incubator at 37°C and 5% CO^2.

Cell Identification

Hematoxylin-eosin (HE) staining and toluidine blue staining were used to observe the cell morphology. For immunofluorescence staining, cells were fixed with 4% paraformaldehyde for 20 min, infiltrated with 0.5% Triton X-100 solution (Solarbio, China) for 30 min, and incubated with 5% goat serum (Solarbio, China) for 30 min at room temperature. Next, collagen II and aggrecan (Affinity Biosciences, Nanjing, China) were added and incubated overnight at 4°C. Following

incubation, a fluorescent secondary antibody (EARTHOX, San Francisco, CA, USA) was added and incubated for 60 min at 37°C protected from light, before adding DAPI staining solution (Beyotime, Nanjing, China) for 5 min at room temperature protected from light. Finally, the cells were washed five times with phosphate buffered saline (PBS) solution, an anti-fluorescence quenching sealer (Solarbio, China) was used to seal the slices, and the slices were observed and photographed using an inverted fluorescence microscope (Olympus, Japan).

Cell Viability Assay

The cell viability was measured using a CCK-8 kit (Dojindo, Japan). After treatment, the cells were collected via digestion, re-suspended, and adjusted to a cell density of 1.0×10^5/mL; then, 100 μL cells were inoculated into 96-well cell culture plates (6 wells per group). Subsequently, 10 μL of CCK-8 solution was added to each well and incubated in an incubator for 1–4 h. After incubation, the absorbance was measured at 450 nm by an enzyme marker (Bio Tek Instruments, USA).

Flow Cytometry Analysis

The Annexin V-FITC/PI Apoptosis Detection kit (Vazyme Biotech, Nanjing, China) was used to detect the rates of apoptosis. Set three samples for each group. After treatment, the cells were digested and collected before adding to 1 × binding buffer 100 μL and gently blown well to a single-cell suspension. For the control and experimental groups, 5 μL Annexin V-FITC and 5 μL PI staining solution were added and gently blown; for the Annexin-V group, 5 μL Annexin V-FITC was added; and for the PI group, 5 μL PI staining solution was added and incubated for 10 min at room temperature, protected from light. Finally, 400 μL of 1 × binding buffer was added, mixed gently, and assayed using flow cytometry (Beckman, USA).

Apoptosis Model Construction

The apoptosis rate was detected after applying a pressure of 1.0 MPa to NPCs for 12 h, 24 h, and 48 h using a homemade cell pressurization device (Figure 1). The NPCs were incubated in an air-free environment to exclude the effect of increased CO_2 solubility on the pH of the medium due to increased air pressure.

Measurement of ROS

ROS were detected using a ROS assay kit (Beyotime, Nanjing, China). Briefly, 2',7'-dichlorofluorescin diacetate (DCFH-DA) was diluted with serum-free medium at 1:1000 to a final concentration of 10 μM. After digestion, the cells were collected and suspended in diluted DCFH-DA and incubated at 37°C for 20 min. The cells were washed thrice

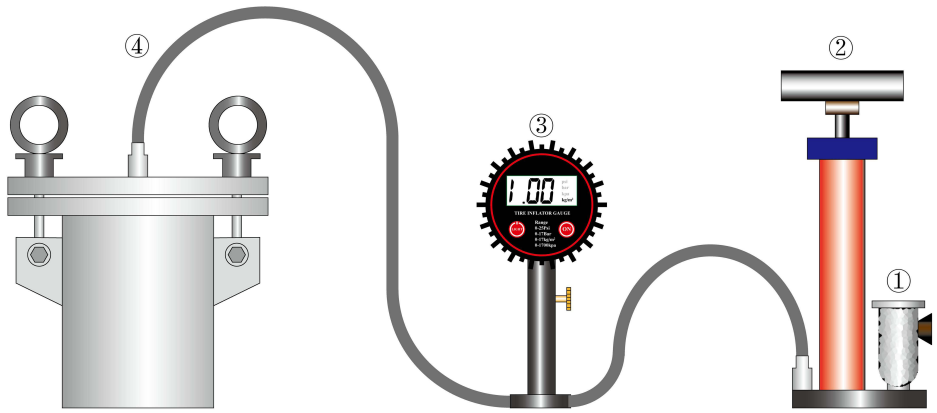

Figure 1 Homemade cell static pressurization device. The composition structure is showing the following: ① Air Filter, ② High pressure pump, ③ Pressure Gauges, and ④ Pressure bin.

with serum-free medium. Rosup was added to the positive control wells as a positive control. After adjusting the density of cells to 1.0×10^8/mL, they were inoculated into a 96-well fluorescent enzyme labeling plate (100 μL per well, 6 wells per group). Various fluorescence intensities were detected using a fluorescent enzyme-linked immunosorbent assay (ELISA) (BioTek Instruments, USA) (ELISA parameters: 488 nm excitation wavelength, 525 nm emission wavelength).

TUNEL Fluorescent Staining

One-step TUNEL Apoptosis Detection Kit (Beyotime, Nanjing, China) was used for TUNEL fluorescence staining. Briefly, the cells were fixed in 4% paraformaldehyde for 30 min after treatment and 0.3% Triton X-100 PBS was added and incubated at 25°C for 5 min. The cells were washed twice with PBS and the appropriate amount of TUNEL assay solution was added and incubated for 60 min at 37°C protected from light. Following a further three washes with PBS, the slices were observed using a fluorescence microscope (Olympus, Japan). The excitation wavelength of Cy3 was 550 nm and the emission wavelength was 570 nm.

Western Blot

Cells or tissues were added to RIPA lysate (Beyotime, Nanjing, China) and homogenized on a homogenizer (Jingxin, China) adjusted to 60 Hz for 45s. Cells or tissues were centrifuged at 14,000 g for 5 min and the supernatant was removed. A BCA Protein Quantification Kit (Vazyme Biotech, Nanjing, China) was used to detect the protein sample concentration. After electrophoresis using SDS-PAGE gel and membrane transfer, protein-free fast blocking solution (Epizyme, China) was used for blocking. Subsequently, the blocking solution was aspirated and primary antibody was added and incubated overnight at 4°C. After washing three times, the secondary antibody was added and incubated at room temperature for 1 h. The ECL developer (Vazyme Biotech, Nanjing, China) was added and then developed using a fully automated chemiluminescent image analysis system (Tanon, China). The grayscale values of each group of bands were analyzed using ImageJ software. The following antibodies were used: aggrecan antibody, collagen II antibody, Nrf2 antibody, phosphorylated Nrf2 antibody, beta actin antibody (all Affinity Biosciences, China); anti-heme oxygenase 1 antibody (Abcam, Cambridge, UK); and the phospho-MAPK family antibody sampler kit and MAPK family antibody sampler kit (Cell Signaling Technology, Danvers, MA, USA).

IDD Model

30 eight-week-old SD rats were used in animal experiment. The rats were randomly divided into four groups (n=6 for each group). As shown in Figure 2A–D, after fixation of SD rats, the middle of Co5 and Co7 vertebrae were X-rayed and positioned as puncture points. Next, 75% alcohol was used to disinfect the caudal vertebrae of the rats, and 5% lidocaine injection was used for local anesthesia. After one disc was snapped into the root of the caudal vertebra, an 0.8-mm kerf needle was used to punch perpendicular to the puncture point of the Co5 vertebra, and an 0.8-mm kerf needle was used to punch perpendicular to the puncture point of the Co7 vertebra and snapped into one disc. Three nuts were threaded into the disc from the proximal end to the distal end, and three springs were installed at the end of the nut followed by a disc. A metal spacer was installed at the end of each nut and screwed onto the nut. The disks were rotated appropriately so that the kerf pins fell into the slots in the disks. The kerf pins were cut off beyond the disk and the nut was rotated to compress the spring to the appropriate length (x) according to the spring's elasticity coefficient (k = 4000 N/m), the diameter of the rat's tailbone (d = 5 mm), and the pressure to which the IVD was subjected (P = 1.0 MPa). The spring compression length was calculated using the following formula: $x = Pm/k$ where P is the pressure, m is the transverse area of the vertebral body, and k is the spring elasticity coefficient. For 3 days after surgery, SD rats were given daily intramuscular injections of penicillin to prevent infection and were disinfected caudally with iodophor. If the rats showed signs of infection, they were removed from the experiment. The spring length was checked daily and adjusted promptly in the event of any change.

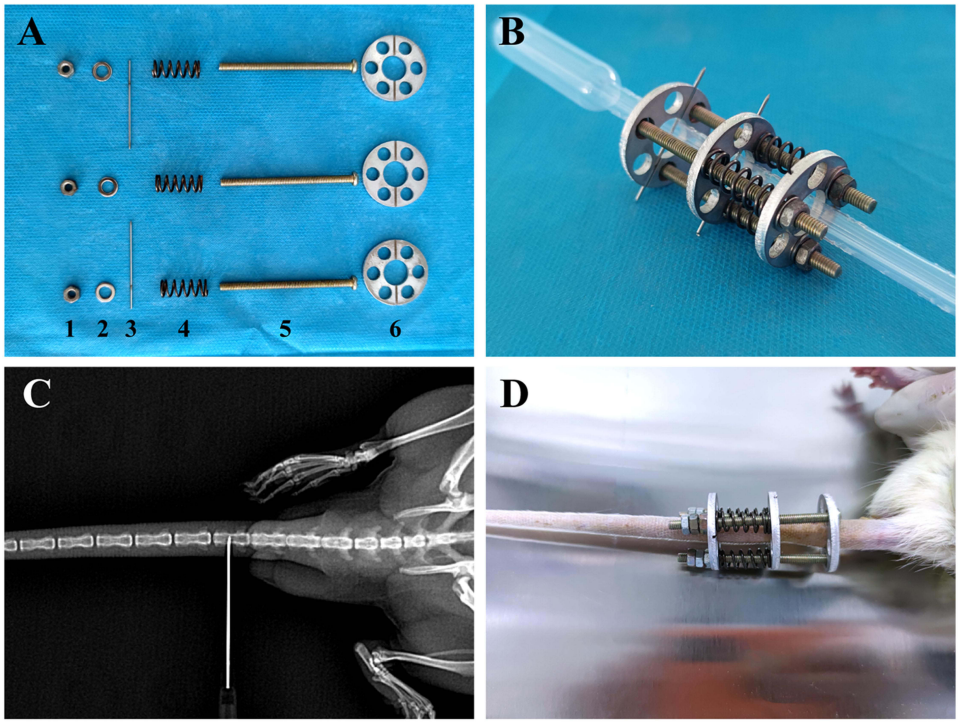

Figure 2 Self-made rat tailbone compression device. (**A**) Components of the compression device: 1, screw; 2, spacer; 3, kerf needle; 4, spring; 5, screw; and 6, aluminum alloy disc. (**B**) Assembly diagram of the compression device. (**C**) X-ray positioning. (**D**) Complete installation of the compression device.

Safranine O-Fast Green FCF Cartilage Stain

For staining with the Modified Safranine O-Fast Green FCF Cartilage Stain Kit (Solarbio, China), the IVD paraffin sections were first dewaxed in xylene for 5–10 min, before replacing with fresh xylene and dewaxing again for 5–10 min, anhydrous ethanol for 5 min, 90% ethanol for 2 min, 80% ethanol for 2 min, 70% ethanol for 2 min, and distilled water for 2 min. Finally, the sections were placed in freshly prepared Weigert staining solution for 3–5 min before washing with water. The sections were quickly washed with a weak acid solution for 10–15 s to remove the residual solid green and then dried. The sections were then immersed in red staining solution for 5 min, before dehydrating in 95% ethanol for 2–3 s, anhydrous ethanol for 2–3 s, and anhydrous ethanol for 1 min. Xylene was used to make the slices transparent, and neutral gum was used to seal the film after.

Medicines Involved

Andrographolide, N-acetylcysteine (ROS inhibitor), Zinc protoporphyrin (ZnPP) (Competitive HO-1 inhibitor), tert-butylhydroquinone (TBHQ) (A widely used Nrf2 activator), retinoic acid (RA) (Inhibition of transcription factor Nrf2 by activation of retinoic acid receptor), ASTX029 (An effective dual ERK1/2 inhibitor), SP600125 (ATP-competitive JNK inhibitor), and TAK-715 (An effective inhibitor of p38 MAPK) were purchased from MedChemExpress (Monmouth Junction, NJ, USA). Details of the medicines are in the Supplementary Material.

Statistical Analysis

All experimental results were analyzed using SPSS 27.0 statistical software for data analysis, and GraphPad Prism 6 software was applied for statistical plotting. A Shapiro–Wilk test combined with a normal Q-Q plot was used to test the distribution of the data. For quantitative data, a one-way analysis of variance (ANOVA) was used, followed by a post-hoc test using either the Bonferroni test or the Tamheiny test. When the sample size is less than 5, the Permutation tests in the non-parametric test were used. The measurement data are expressed as the mean ± standard deviation. Differences were considered statistically significant at $P < 0.05$.

Results

NPC Phenotype

Under microscopy, NPCs were short rod-shaped, triangular, polygonal, short pike shaped, and connected into sheets. The nucleus was blue and the cytoplasm was pink after HE staining. After toluidine blue staining, the acidic aggrecan in the cytoplasm was colored blue, with darker coloration observed closer to the nucleus. In immunofluorescence staining, collagen II and aggrecan showed red and green fluorescence, respectively, with stronger fluorescence intensity observed closer to the nucleus, while the nucleus showed blue fluorescence (Figure 3).

NPC Apoptosis Model

To exclude the effect of increased CO_2 solubility on the pH of the medium due to increased air pressure, no significant changes in cell viability were observed after NPCs were incubated in an air-free environment for 24 h and 48 h ($P > 0.05$) (Figure 4A, Table S1). The apoptosis rates were detected after applying a pressure of 1.0 MPa to NPCs for 12 h, 24 h, and 48 h using a homemade cell pressurization device. When the pressurization time was < 24 h, there was no significant increase in the apoptosis rate ($P > 0.05$). When the pressurization time was ≥ 24 h, the apoptosis rate increased significantly ($P < 0.05$), and increased continuously with the increase in pressurization time (Figure 4B and C, Figure S1, Table S2). A pressure treatment of 1.0 MPa for 24 h was selected as the condition for constructing the NPC apoptosis model.

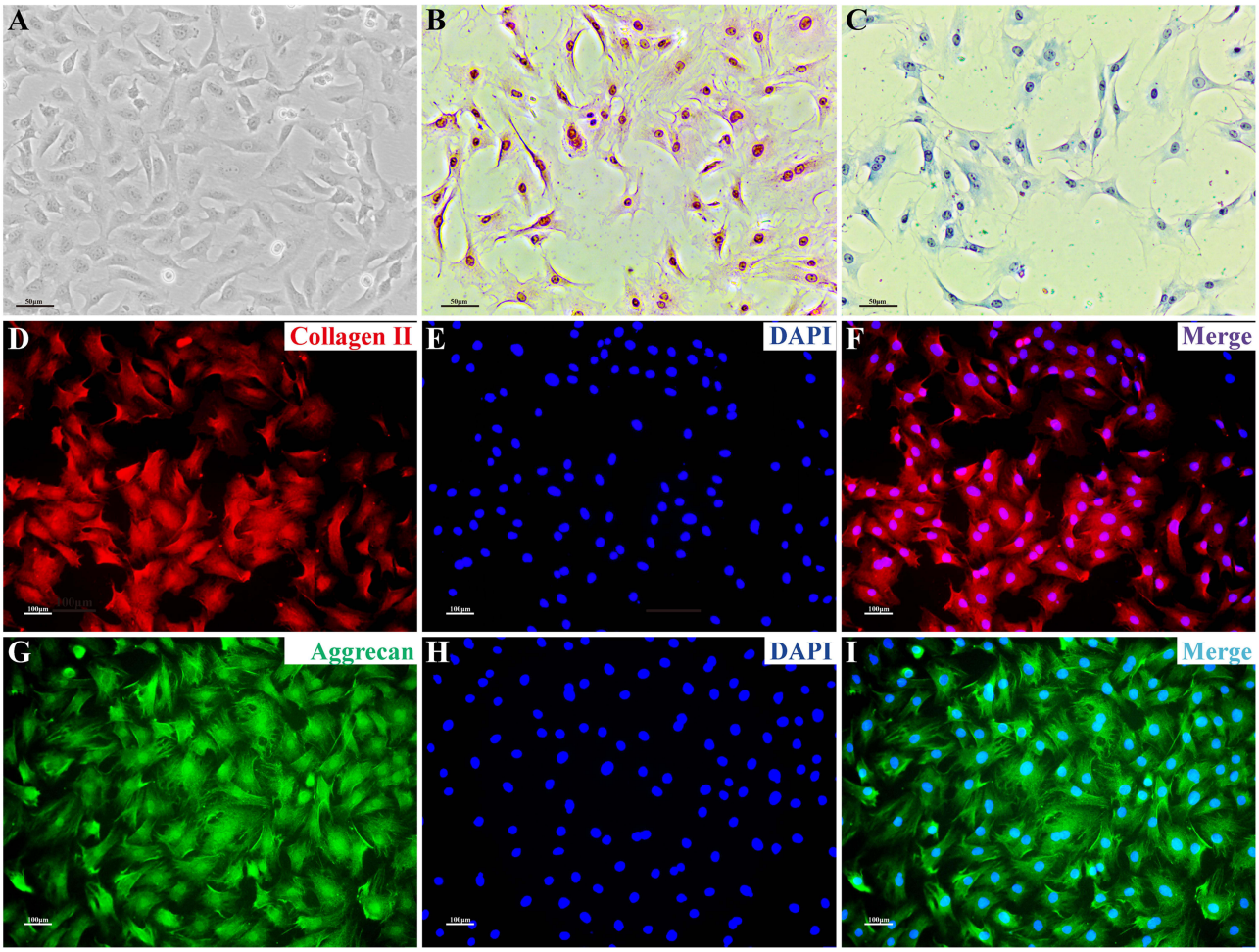

Figure 3 NPC phenotype. (**A**) Morphological observation of NPCs. (**B**) NPCs stained with H&E; the nuclei are blue and the cytoplasm is pink. (**C**) After toluidine blue staining, the acidic aggrecan in the cytoplasm was visualized by blue staining, with the darker color observed closer to the nucleus. (**D–I**) Immunofluorescence staining: collagen II and aggrecan showed red and green fluorescence, respectively, with stronger fluorescence intensity observed closer to the nucleus; the nucleus showed blue fluorescence. Scale bars: 50 μm in (**A–C**), 100 μm in (**D–I**).
Abbreviation: NPC, nucleus pulposus cell.

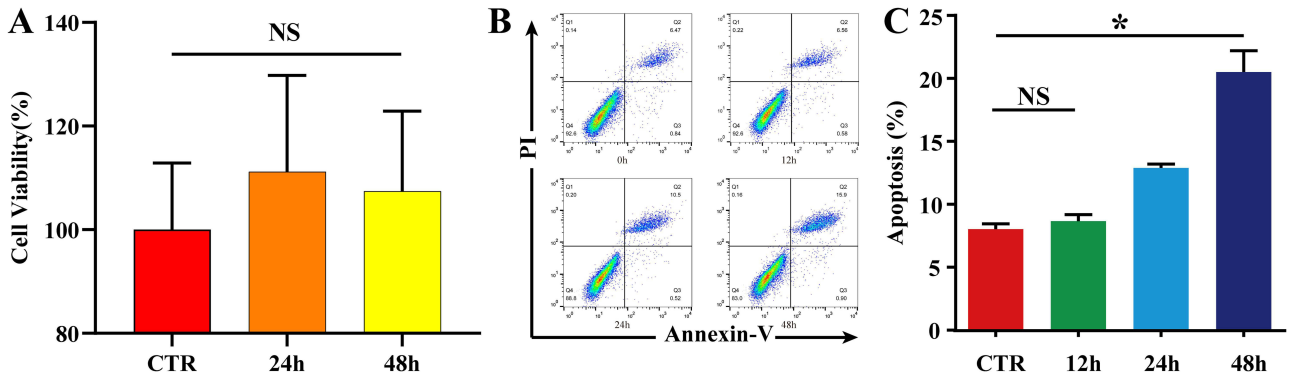

Figure 4 NPC apoptosis model. (**A**) To exclude the effect of increased CO_2 solubility on the pH of the medium due to increased air pressure, NPCs were incubated in an air-free environment for 0 h, 24 h, and 48 h, and cell viability was detected using a CCK-8 kit. The results are expressed as the mean ± standard deviation, n=5 for each group. The data showed no significant change in cell proliferation viability in the 24 h and 48 h groups compared to the CTR group ($P > 0.05$). (**B** and **C**) Flow cytometric detection of the NPC apoptosis rate; NPCs were placed in a pressure chamber and cultured in a pressure environment of 1.0 MPa for 0 h, 12 h, 24 h, and 48 h, before detecting the apoptosis rate using an Annexin V-FITC/PI Apoptosis Detection Kit. The results are expressed as the mean ± standard deviation, n=5 for each group. The apoptosis increased significantly when the pressurization time was ≥ to 24 h ($P < 0.05$, compared to the CTR group), and increased continuously with the increase in pressurization time. *$P < 0.05$.

Abbreviations: NPC, nucleus pulposus cell; CTR, control; NS, non-significant.

ADR Protects NPCs from the Damage Caused by Static Mechanical Pressure

The CCK-8 kit was used to detect the effect of ADR on the viability of NPCs induced by static mechanical pressure. Considering that cell viability was not affected when the ADR concentration was < 15 μM, 10 μM was used as the optimal concentration to detect the protective effect of ADR (Figure 5A, Table S3). Cell viability decreased to 74.14% ($P < 0.01$) following the culture of NPCs in a 1.0 MPa environment for 24 h. When pretreated with ADR or N-acetylcysteine (NAC) for 8 h, the cell viability decreased to 84.09% and 87.24% respectively. Cell viability was significantly increased in the ADR and NAC groups compared to the PRE group ($P < 0.01$) (Figure 5B, Table S4). The ROS content and apoptosis rate were significantly increased in the PRE group ($P < 0.01$). Although cell viability was still significantly increased after pretreatment with ADR or NAC for 8 h compared to the CTR group ($P < 0.01$), it was significantly decreased in the ADR and NAC groups compared to the PRE group ($P < 0.01$) (Figure 5C–E, Figure S2, Table S5 and S6). Similar results were observed during TUNEL fluorescence staining (Figure 5F).

ADR Induced the Expression of Heme Oxygenase-1 (HO-1) in NPCs to Resist Static Mechanical Pressure-Induced Damage

ADR induced the expression of HO-1 and p-Nrf2 time-dependent ($P < 0.05$) and had no significant effect on the expression of total Nrf2 ($P > 0.05$). (Figure 6A–D, Table S7). Although static mechanical pressure could promote the expression of HO-1, the difference was not statistically significant ($P > 0.05$), and the promotion of HO-1 expression by ADR could be reversed using ZnPP (Figure 6E and F, Table S8). Static mechanical pressure can lead to the accumulation of ROS in NPCs, and when NPCs were pretreated with ADR to promote HO-1 expression, the accumulation of ROS was significantly inhibited; this protective effect could be reversed by the HO-1 inhibitor (Figure 6G, Table S9).

ADR Upregulates HO-1 Expression via the MAPK/Nrf2 Signaling Pathway

NPCs were treated with tert-butylhydroquinone (TBHQ) (Nrf2 agonist) or retinoic acid (RA) (Nrf2 inhibitor) for 6 h followed by ADR for 8 h. The results of Western blot assay showed that both ADR and TBHQ promoted the expression of p-Nrf2 and HO-1 ($P < 0.05$). Treatment with RA reversed the effect of ADR and significantly inhibited the expression of p-Nrf2 and HO-1 ($P < 0.05$) (Figure 7A–D, Table S10). According to the experimental grouping, NPCs were treated with ASTX029 (Erk1/2 inhibitor), SP600125 (JNK inhibitor), and TAK-715 (p38 inhibitor) for 6 h followed by ADR for 8 h. Western blot assay showed that although ADR could promote the expression of p-p38, p-Erk1/2, p-JNK, p-Nrf2, and HO-1 ($P < 0.05$), the expression of p-Nrf2 and HO-1 was significantly increased after activation of the p38 signaling pathway alone compared to that following the activation of the Erk1/2 or JNK signaling pathway alone ($P < 0.05$).

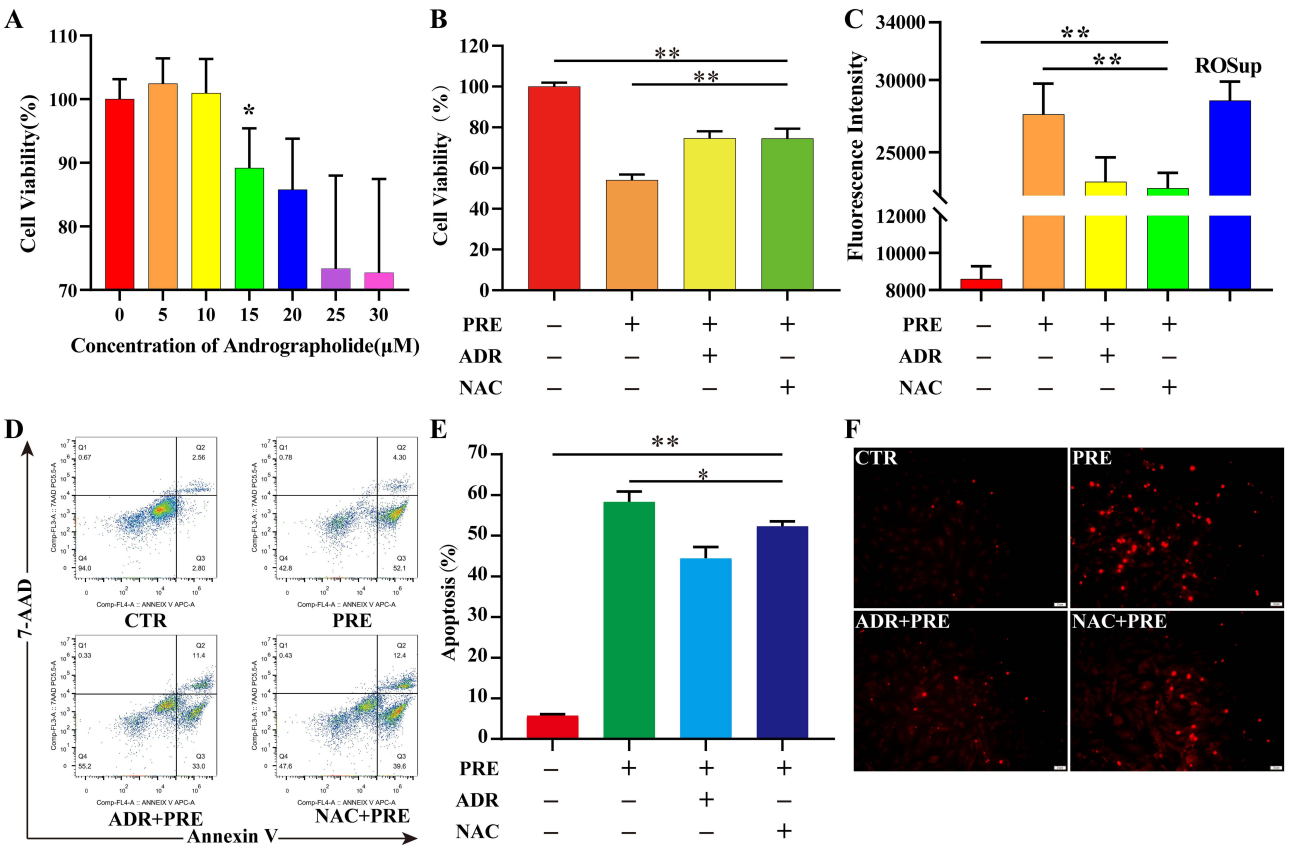

Figure 5 ADR protects NPC from static mechanical pressure-induced damage. (**A**) Effect of ADR on NPC viability. NPCs were cultured in medium with ADR concentrations ranging from 0 μM to 30 μM for 24 h, and cell viability was measured using the CCK-8 kit; the results are expressed as the mean ± standard deviation, n=6 for each group. A significant decrease in cell viability was observed at ADR concentrations > 10 μM ($P < 0.05$). NPCs were pretreated with or without ADR or NAC for 8 h and then incubated in a 1.0 MPa environment for 24 h. (**B**) Cell viability was assayed using the CCK-8 kit. The results are expressed as the mean ± standard deviation, n=6 for each group. The cell viability was significantly inhibited by static mechanical pressure ($P < 0.01$), but significantly improved after pretreatment with ADR or NAC ($P < 0.01$). (**C**) ROS content was measured using ROS assay kit. The results are expressed as the mean ± standard deviation, n=6 for each group. The ROS content was significantly increased by static mechanical pressure ($P < 0.01$), but significantly decreased after pretreatment with ADR or NAC ($P < 0.01$). (**D** and **E**) Detection of apoptosis using the Annexin V-FITC/PI Apoptosis Detection Kit. The results are expressed as the mean ± standard deviation, n=3 for each group.The apoptosis rate was significantly increased by static mechanical pressure ($P < 0.01$), but significantly decreased after pretreatment with ADR or NAC ($P < 0.05$). (**F**) Apoptosis was detected again using TUNEL fluorescent staining. Sporadic nuclear fixation was observed in the control group, which showed red fluorescent highlights along with TUNEL assay solution. The number of red fluorescent bright spots increased significantly increased in the pressure group, but significantly decreased after pretreatment with ADR or NAC. *$P < 0.05$, **$P < 0.01$.
Abbreviations: ADR, andrographolide; NPC, nucleus pulposus cell; ROS, reactive oxygen species; NAC, N-acetylcysteine.

Moreover, ADR could still upregulate the expression of p-Nrf2 and HO-1 ($P < 0.05$) when p38, Erk1/2, and JNK signaling pathways were simultaneously inhibited (Figure 7E–J, Table S11).

ADR Effectively Inhibits Static Mechanical Pressure-Induced IDD

HE and safranine O-fast green FCF cartilage stain showed good morphology of the IVD in the CTR and SOL groups, with a normal intervertebral space height, a neat arrangement of the annulus fibrosus in an annular hierarchy, and no signs of fibrous ring fracture or disorder. The central part of the NP was oval in shape, full in volume, rich in ECM, and its internal collagen II and aggrecan were filled in lattice-like intracellular compartments. NPCs were abundant in the intracellular compartments. The thickness of the upper and lower cartilage endplate was high, and transparent chambers of varying sizes were visible within, which were filled with abundant collagen and cartilage endplate cells. The IVD height was significantly lower in the PRE and EXP groups compared to that in the CTR and SOL groups, and the cartilage endplate was significantly thinner. The size of the hyaline compartment within the cartilage endplate was significantly reduced and the collagen content was significantly decreased, with inflammatory cell infiltration observed inside. In the PRE group, the fibrous rings were disorganized, with fissures and fractures inside the rings. Furthermore, the NP was heavily resorbed, leaving only a small portion of the volume, with no internal cellular structure, a transparent

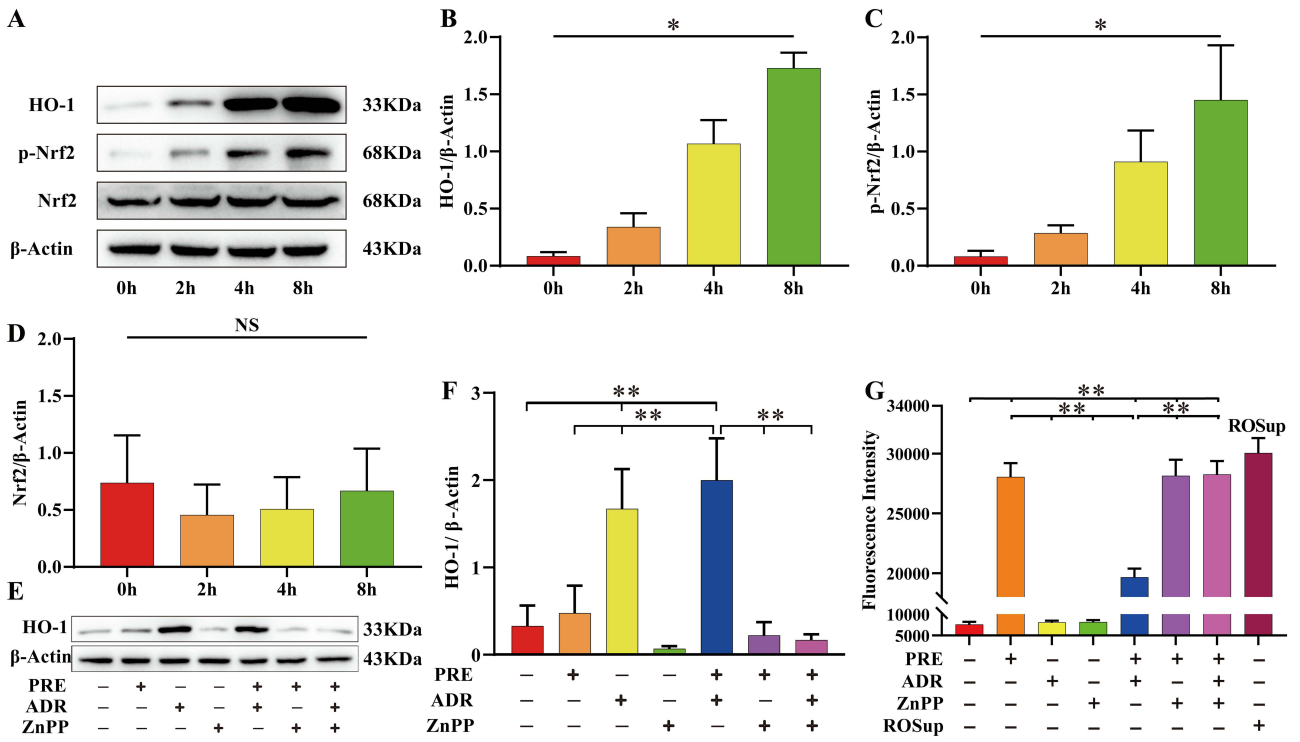

Figure 6 ADR induced the expression of HO-1 in NPC to resist static mechanical pressure-induced damage. (**A–D**) Western blot was used to detect the effect of ADR on the expression of HO-1 and Nrf2. Total proteins were extracted from NPCs after various culture periods (0 h, 2 h, 4 h, and 8 h) using an ADR concentration of 10 μM and β-Actin as a reference. ADR induced the expression of HO-1 and p-Nrf2 in a time-dependent manner ($P < 0.05$) and had no significant effect on the expression of total Nrf2 ($P > 0.05$). Values measured are presented as the mean ± standard deviation, n=3 for each group. (**E–G**) To clarify whether the cytoprotective effect of ADR was achieved by inducing the expression of HO-1, we used ADR or ZnPP to treat NPC for 8 h, followed by the application, or not, of 1.0 MPa static pressure for 24 h. The ROS content was significantly increased in the PRE group compared to the CTR group ($P < 0.05$). Data are expressed as the mean ± standard deviation, n=6 for each group. ADR promoted HO-1 expression and inhibited ROS accumulation in the ADR + PRE group compared to the PRE group ($P < 0.05$). The upregulation of HO-1 expression by ADR was reversed by ZnPP in the ADR + ZnPP + PRE group compared to the ADR + PRE group ($P < 0.05$), resulting in a significant increase in ROS ($P < 0.05$). Values measured are presented as the mean ± standard deviation, n=3 for each group. *$P < 0.05$, **$P < 0.01$.

Abbreviations: ADR, andrographolide; NPC, nucleus pulposus cell; ROS, reactive oxygen species; ZnPP, Zinc protoporphyrin (HO-1 inhibitor); CTR, control; PRE, pressure; HO-1, heme oxygenase-1; Nrf2, NF-E2-related factor 2; NS, non-significant.

appearance, and no ECM coloring, such as collagen II and aggrecan. In the EXP group, although the fibrous rings were also disorganized, fissured, and broken, the volume of myeloid tissue was significantly larger than that of the pressure group, suggesting that the degeneration of myeloid tissue in the EXP group was less than that in the PRE group (Figure 8A–H). The results of Western blot showed that static mechanical pressure could significantly inhibit the expression of collagen II and aggrecan, and when treated with ADR, it could significantly promote the expression of HO-1, p-Nrf2, collagen II, and aggrecan (Figure 8I–N, Table S12).

Discussion

In this study, we explored the molecular mechanisms by which ADR inhibits static mechanical stress-induced IDD. Our results suggest that ADR inhibits the accumulation of ROS through the MAPK/Nrf2/HO-1 signaling pathway and upregulates the expression of the antioxidant enzyme HO-1 to suppress IDD.

ROS are by-products of eukaryotic mitochondrial energy metabolism and can be broken down by intracellular reducing agents or antioxidant enzymes (eg, superoxide dismutase, catalase, glutathione peroxidase, and thioredoxin reductase) to maintain low levels in the body. Studies have shown that excess ROS can damage DNA and organelle membranes, and cause protein misfolding, leading to various diseases.[18] Our results showed that treatment of NPCs with a static mechanical pressure of 1.0 MPa for 24 h not only significantly inhibited the viability of NPCs (Figure 3B), but also significantly increased apoptosis and ROS accumulation (Figure 3C–F). Therefore, we speculate that static mechanical pressure may affect NPC energy metabolism, leading to ROS accumulation, which in turn leads to increased

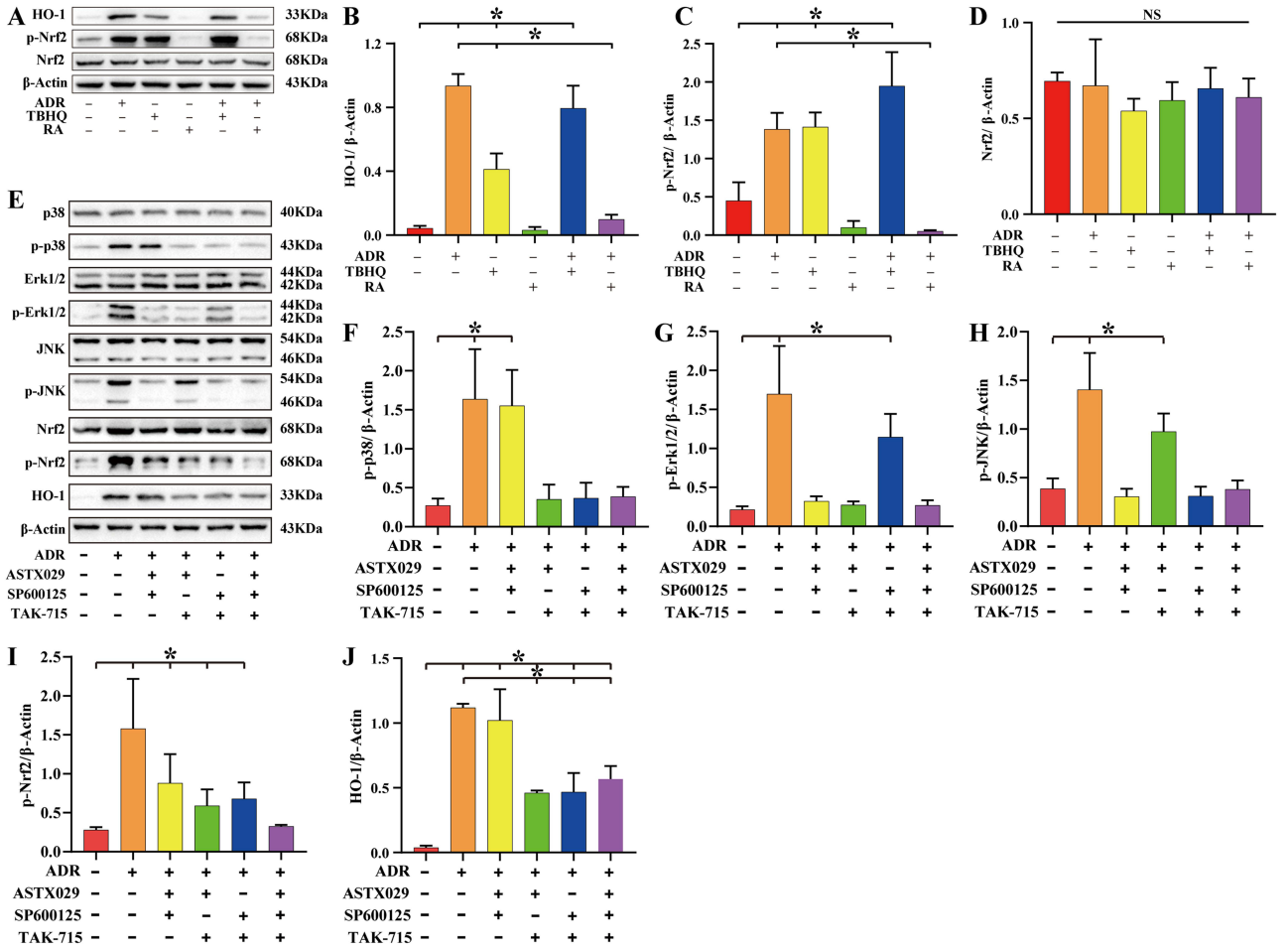

Figure 7 ADR upregulates HO-1 expression via the MAPK/Nrf2 signaling pathway. (**A**–**D**) To clarify whether ADR upregulated HO-1 expression by activating Nrf2, we treated NPCs with TBHQ (Nrf2 agonist) or RA (Nrf2 inhibitor) for 6 h followed by ADR for 8 h. Total proteins were extracted for Western blot assay, and β-Actin was used as an internal reference. The results showed that ADR and TBHQ had similar effects, both promoting the expression of p-Nrf2 and HO-1 ($P < 0.05$). RA treatment reversed the effect of ADR and significantly inhibited the expression of p-Nrf2 and HO-1. (**E**–**J**) To clarify whether MAPK (p38, Erk1/2, and JNK) are upstream signaling pathways of Nrf2, NPCs were treated with ASTX029, SP600125, or TAK-715, followed by ADR for 6 h. Western blot showed that ADR could activate the p38, Erk1/2, and JNK signaling pathways and upregulate the expression of p-Nrf2 and HO-1 ($P < 0.05$). Following simultaneous inhibition of the p38, Erk1/2, and JNK signaling pathways, ADR still upregulated the expression of p-Nrf2 and HO-1 ($P < 0.05$). Values measured are presented as the mean ± standard deviation, n=3 for each group. *$P < 0.05$.
Abbreviations: ADR, andrographolide; TBHQ, Nrf2 agonist; RA, Nrf2 inhibitor; ASTX029, Erk1/2 inhibitor; SP600125, JNK inhibitor; TAK-715, p38 inhibitor; HO-1, heme oxygenase-1; Nrf2, NF-E2-related factor 2; MAPK, mitogen-activated protein kinase; NS, non-significant differences.

apoptosis and decreased viability of NPCs. The reason for this may be related to the activation of mechanically gated Piezo1 ion channels by static mechanical pressure.[19] Indeed, it has been shown that mechanical pressure can induce a change in the conformation of mechanically gated Piezo1 ion channels from a closed to an open state. The large inward flow of extracellular calcium ions decreases the potential difference between the inner and outer mitochondrial membranes in the cell and causes damage to the mitochondrial membrane. Mitochondrial energy metabolism is disturbed and excessive ROSs are produced, exceeding the working capacity of the intracellular redox system, which eventually leads to DNA damage, organelle membrane destruction, and impaired protein synthesis, causing apoptosis or cell death.[20] Cao et al also showed that stress can induce senescence and apoptosis in human NPCs by activating Piezo1 channels to increase intracellular calcium levels, leading to increased ROS and activation of mitochondrial and endoplasmic reticulum apoptotic pathways. Inhibition of Piezo1 activity attenuates oxidative stress induced by increased stress and inhibits NPC senescence and apoptosis.[21] Given the above findings, the most fundamental measure to inhibit IDD is to remove the effects of external mechanical stress on the disc. However, activities such as rotation, bending, weight bearing, and stretching of the spine cause various deformations to occur in the IVD, which causes the NP to be in a constant state of high pressure and deformation. Even when the IVD is not under any pressure, the pressure within the

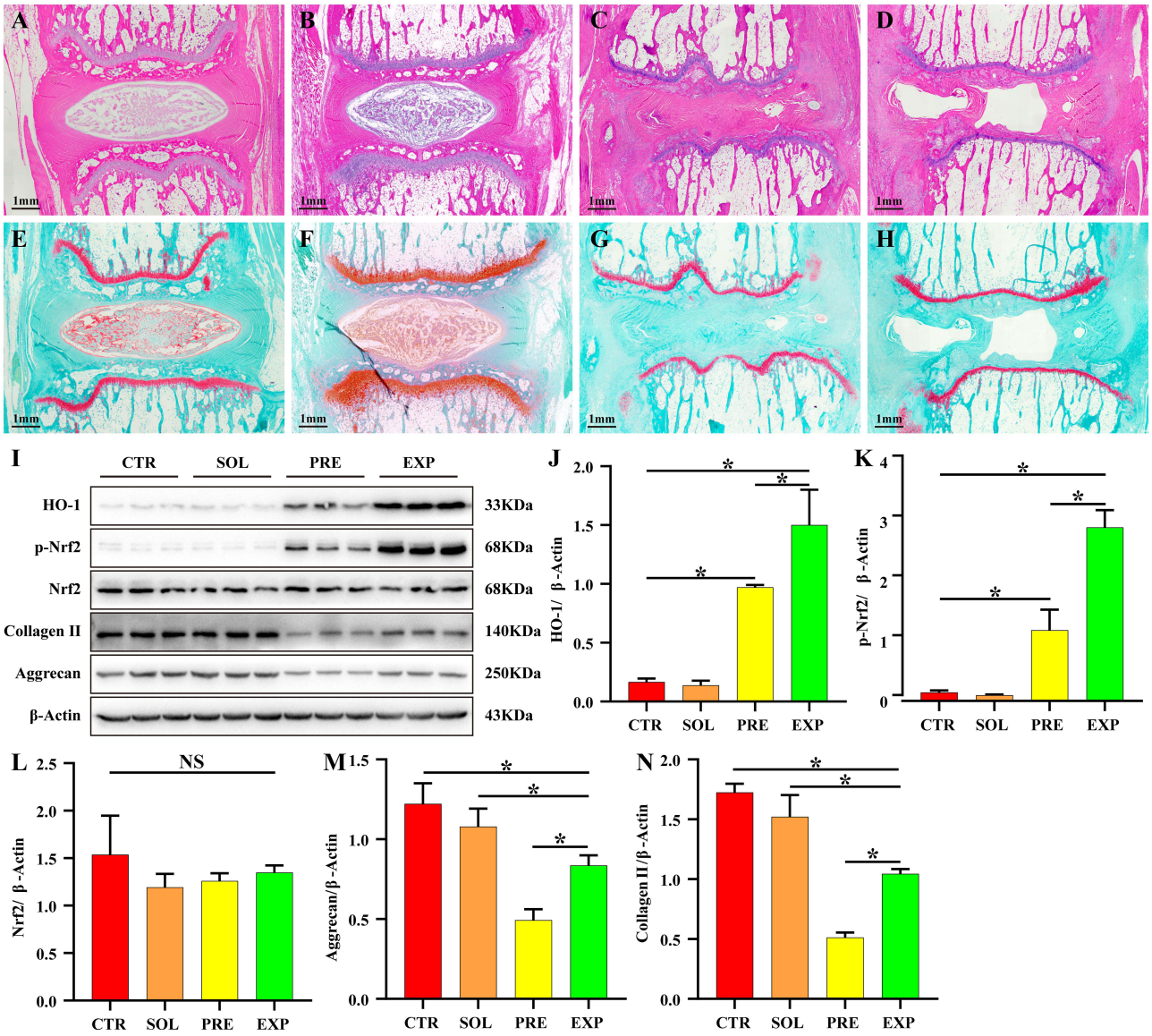

Figure 8 ADR effectively inhibits static mechanical pressure-induced IDD. H&E staining of sagittal sections of the IVD showed that the disks in the CTR group (**A**) and SOL group (**B**) had good morphology, with a normal intervertebral space height. Additionally, the fibrous rings were pinkish in color and neatly arranged in an annular stratification without fibrous ring fracture or disorder. The central part of the nucleus pulposus was blue-purple and oval in shape, full in volume, and rich in extracellular matrix, and its internal type II collagen and aggregated proteoglycans were filled in lattice-like intracellular chambers. The nucleus was stained blue and the cell pulp was stained pink. The thickness of the upper and lower cartilage endplate was higher, and transparent chambers of different sizes were visible within the cartilage endplate and filled with abundant collagen and cartilage endplate cells. The disc height was significantly lower in the PRE group (**C**) and the EXP group (**D**) compared to the control and solvent groups, and the cartilage endplate was significantly thinner. The volume of the hyaline compartment within the cartilage endplate was significantly reduced, and the collagen content was significantly decreased, with inflammatory cell infiltration observed within it. In the PRE group, the fibrous rings were disorganized, with fissures and fractures inside the rings, and the nucleus pulposus was heavily resorbed, leaving only a small portion of the volume, with no internal cellular structure and a transparent appearance. In the EXP group, the volume of the nucleus pulposus tissue was significantly larger than that in the pressure group, although the fibrous rings were also disorganized, fissured, and fractured. The sagittal sections of intervertebral discs stained with safranine O-fast green FCF cartilage (**E**–**H**), (**E**) CTR group, (**F**) SOL group, (**G**) PRE group, (**H**) EXP group) showed similar results to those of **H&E** staining. (**I**–**N**) The expression of HO-1 and p-Nrf2 was significantly increased ($P < 0.05$) and the expression of collagen II and aggrecan was significantly decreased ($P < 0.05$) in the PRE and EXP groups compared to those in the CTR and SOL groups. HO-1, p-Nrf2, collagen II, and aggrecan expression were significantly increased in the EXP group compared to the PRE group ($P < 0.05$). Values measured are presented as the mean ± standard deviation, n=3 for each group. *$P < 0.05$.

Abbreviations: ADR, andrographolide; IDD, intervertebral disc degeneration; IVD, intervertebral disc; CTR, control; PRE, pressure; SOL, solvent; EXP, experimental; HO-1, heme oxygenase-1; Nrf2, NF-E2-related factor 2.

IVD is not zero;[8] therefore, one can only re-treat to inhibit Piezo1 activation.[21] To date, the only identified inhibitor or antagonist of Piezo1 is Dooku1, which functions as a selective, endogenous Piezo1 channel antagonist; however, there are currently no studies or evidence of its application in the clinic.[22] Therefore, the feasible solution is to suppress IDD by reducing the accumulation of ROS due to static mechanical pressure.

ADR has powerful antioxidant activity, which is mediated by directly neutralizing free radicals or indirectly, by protecting mitochondrial integrity, inhibiting pro-oxidant enzymes, and/or activating antioxidant enzymes.[23] Our results showed that when NPCs were pretreated with ADR or NAC, the ROS content and rates of apoptosis were significantly reduced, and the cell viability was improved (Figure 3B–F). These results suggest that the use of ADR to inhibit ROS accumulation in NPC is an effective method to suppress static mechanical stress leading to IDD.

HO-1 is the rate-limiting enzyme for heme degradation and can be induced to be expressed by various stimuli, such as oxidative stress, heat shock, UV irradiation, ischemia-reperfusion, heavy metals, bacterial lipopolysaccharides, cytokines, NO, and hemoglobin.[24] HO-1 has antioxidant, anti-inflammatory, and anti-apoptotic activities, as well as the ability to modulate signal transduction, perform immune regulation, and inhibit of adhesion molecule expression. The powerful adaptive response of HO-11 to various stimulators reveals that it may play an important role in preventing inflammatory processes and oxidative tissue damage.[25–27] Indeed, the results of our previous study showed that the upregulation of HO-1 expression using CDDO-EA activation of the Nrf2/HO-1 signaling pathway significantly inhibited oxidative stress injury in NPCs caused by high glucose concentrations.[28] In this study, we found that ADR could upregulate HO-1 expression in a time-dependent manner (Figure 4A–D). To clarify whether ADR exerts antioxidant effects through upregulation of HO-1, we treated NPCs with ADR and/or ZnPP followed by imposing a static mechanical pressure of 1.0 MPa. The results showed that static mechanical stress induced ROS accumulation in NPCs, while pretreatment with ADR significantly up-regulated HO-1 expression and inhibited ROS accumulation. When NPCs were pretreated with both ADR and ZnPP, not only the upregulation of HO-1 expression by ADR was reversed, but also the intracellular ROS accumulation was significantly increased. These findings suggest that ADR can inhibit ROS accumulation by regulating HO-1 expression in addition to directly neutralizing free radicals.

External stimuli and endogenous free radicals can both damage cellular components; to counteract these negative effects, the body develops a complex oxidative stress response system to mitigate cell damage.[29] NF-E2-related factor 2 (Nrf2), a key transcription factor that regulates resistance to oxidative stress, plays an important role in the antioxidant response of the body; therefore, Keap1-Nrf2 has become an important therapeutic target in cancer, neurodegenerative disease, autoimmune diseases, and inflammation.[30]

NRF2 belongs to the Cap'n'collar (CNC) transcription factor family, consisting of multiple Neh domains (Neh1, Neh2, Neh3, Neh4, Neh5, and Neh6), where the Neh2 structural domain mediates the interaction with Keap1 through DLG and ETGE motifs.[31] Keap1 is a Cullin3 (Cul3)-dependent substrate-bridging protein of the E3 ubiquitin ligase complex that assembles with Cul3 and Rbx1 to form a functional E3 ubiquitin ligase complex (Keap1-Cul3-E3), which in turn regulates Nrf2.[32] Keap1 contains three functional domains, including BTB, IVR, and Kelch/DGR. Under normal physiological conditions, the Keap1-Cul3-E3 ubiquitin ligase targets multiple lysine residues bound to the Neh2 structural domain at the N-terminal end of Nrf2 (located between the DLG and ETGE motifs) and promotes ubiquitination. The ubiquitinated Nrf2 is delivered to the 26S proteasome for degradation.[33] In contrast, exposure to ROS induces modification of specific cysteine residues in Keap1, causing a conformational change in the Keap1-Cul3-E3 ubiquitin ligase and inhibiting Nrf2 ubiquitination. Phosphorylated Nrf2 translocates to the nucleus and induces the expression of a series of cytoprotective genes, including HO-1, superoxide dismutase (SOD), cadherin, and cadherin dismutase, through heterodimerization with small Maf (sMAF) proteins bound to the ARE/EpRE (antioxidant response element/electrophilic response element) of target genes, including SOD, catalase, thioredoxin, peroxiredoxin, glutathione peroxidase, glutathione reductase, glutamine cysteine ligase and glutamine cysteine synthetase, and NAD(P)H quinine oxidoreductase.[34,35]

To reveal whether ADR upregulates HO-1 through the Nrf2 pathway, we used ADR and/or TBHQ or RA to treat NPC for 8 h. The results of Western blot showed that ADR and TBHQ had similar effects in that they both upregulated HO-1 expression by promoting the phosphorylation of Nrf2. When the phosphorylation of Nrf2 was inhibited by RA, the upregulation of HO-1 by ADR was reversed (Figure 5A–D). The above experimental results reveal that ADR exerts antioxidant effects by promoting the phosphorylation of Nrf2 and translocation to the nucleus, activating ARE/EpRE, and thus promoting HO-1 expression.

Mitogen-activated protein kinase (MAPK) is expressed in all eukaryotic cells and its pathway consists of a conserved three-tier kinase pattern, including MAPK kinase (MKK), MAPK kinase (MAP kinase, MKK), and MAPK, ie, the

MAP3K-MAP2K-MAPK chain.[36] The three kinases can be activated sequentially to transmit upstream signals to downstream response molecules through sequential phosphorylation, before participating in numerous important cellular physiopathological processes, such as stress adaptation to the environment and inflammatory responses. As isoforms of MAPK, extracellular regulatory protein kinase (ERK1/2), p38 protein kinase (p38 MAPK), and stress-activated protein kinase (JNK) signaling pathways can regulate cell proliferation and apoptosis by mediating the cellular oxidative stress response, inflammatory response, and cellular metabolism. Several studies have shown that MAPK is an upstream signaling molecule of Nrf2 and promotes the activation of the downstream antioxidant enzyme system by promoting Nrf2 phosphorylation and nuclear translocation.[37–39] We used ASTX029 (ERK1/2 inhibitor), SP600125 (JNK inhibitor), and TAK-715 (p38 inhibitor) according to different groupings to treat NPCs for 6 h followed by ADR for 8 h. The results of Western blot showed that ADR could activate the p38, Erk1/2, and JNK signaling pathways to upregulate the expression of p-Nrf2 and HO-1. However, the expression of HO-1 was significantly higher after activation of the p38 signaling pathway alone compared to that after activation of the Erk1/2 or JNK signaling pathway alone, suggesting that ADR upregulates HO-1 expression mainly through activating the p38 signaling pathway. Moreover, blocking the p38, Erk1/2, and JNK signaling pathways increased p-Nrf2 expression, although not significantly ($P > 0.05$), while HO-1 expression was still significantly increased ($P < 0.05$) (Figure 5E–J). One reason for this is that although the expression trend of HO-1 is consistent with the phosphorylation trend of Nrf2, a small amount of p-Nrf2 can promote a large amount of HO-1 expression. Additionally, we only blocked the MAPK signaling pathway-mediated Keap1-Nrf2 classical activation pathway, when the cellular autophagy-lysosome pathway also plays a key role in mediating oxidative stress. Autophagy is a tightly regulated cellular degradation pathway responsible for the removal of damaged proteins and organelles, including oxidatively damaged proteins and abnormally functioning mitochondria. Dysfunctional autophagy leads to accumulation of the autophagic bridging protein p62; because p62 contains structural domains that interact with other proteins, its accumulation leads to the isolation and loss of function of many binding proteins, including Keap1.

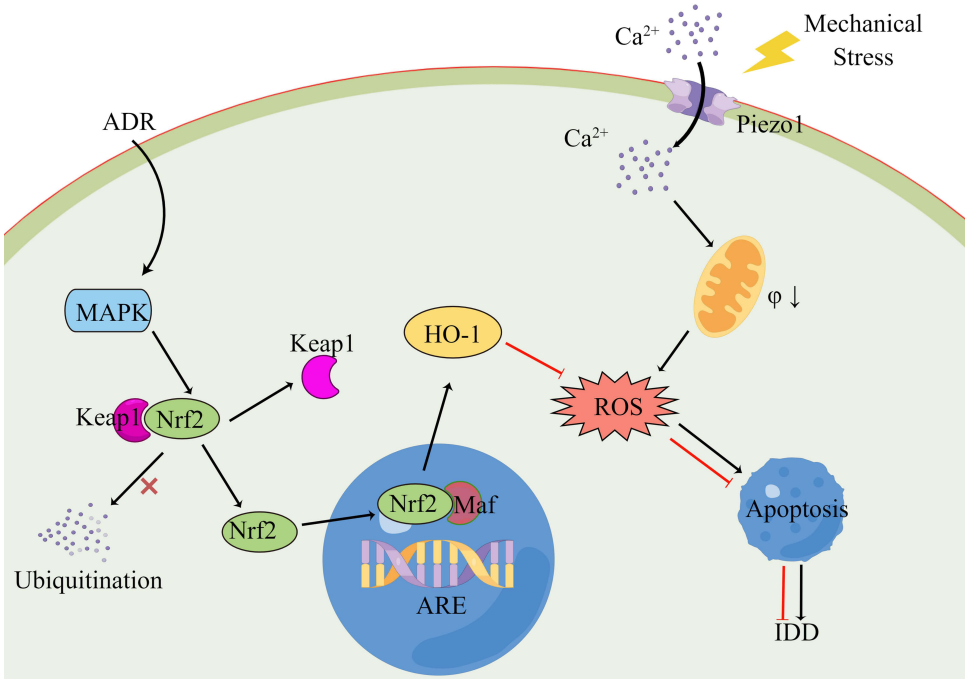

Figure 9 Schematic representation of ADR inhibition of static mechanical pressure-induced apoptosis in NPCs. Mechanical stress can induce a change in the conformation of mechanically gated Piezo1 ion channels from a closed to an open state. The large inward flow of extracellular calcium ions decreases the potential difference between the inner and outer mitochondrial membranes in the NPCs and causes damage to the mitochondrial membrane. Mitochondrial energy metabolism is disturbed and excessive ROSs are produced, exceeding the working capacity of the intracellular redox system, which eventually leads to apoptosis or cell death. ADR can activate the MAPK signaling pathway and inhibit the ubiquitination of Nrf2 by Keap1 to promote Nrf2 phosphorylation and translocation to the nucleus and binding to ARE/EpRE. Ultimately, this induces the expression of antioxidant enzyme systems such as HO-1, inhibits intracellular ROS accumulation, improves NPC viability and inhibits apoptosis.
Abbreviations: ADR, andrographolide; NPC, nucleus pulposus cell; ROS, reactive oxygen species; MAPK, mitogen-activated protein kinase; Nrf2, NF-E2-related factor 2; HO-1, heme oxygenase-1.

Moreover, p62 competes with Nrf2 for binding Keap1, and this interaction allows p62 to sequester Keap1 into the autophagosome, thereby preventing Keap1-mediated degradation of Nrf2 and leading to Nrf2 pathway activation.[40,41] Therefore, ADR may also promote HO-1 expression by regulating the autophagic function of NPCs through the activation of Nrf2 via a non-classical pathway. Taken together, our results demonstrate that ADR can inhibit static mechanical pressure-induced NPC apoptosis by activating the MAPK/Nrf2/HO-1 signaling pathway and upregulating HO-1 expression.

To verify whether ADR can also work in vivo, we injected ADR into the caudal disks of rats with or without ADR and then applied a static mechanical pressure of 1.0 MPa for 1 month. HE and safranine O-fast green FCF cartilage staining showed that the disc height, annulus fibrosus integrity, and alignment were better in the ADR-treated group than in the pressure-only group, and the volume of the NP tissue was significantly larger than that in the pressure group. Additionally, the results of Western blot showed that the expression of p-Nrf2, HO-1, collagen II, and aggrecan were significantly increased after ADR treatment compared to the pressure-only group, suggesting that IDD was significantly reduced after ADR treatment. Moreover, the results of in vivo experiments showed that ADR can indeed inhibit static mechanical pressure-induced IDD through upregulation of HO-1 expression.

Conclusion

Overall, our results suggest that ADR can inhibit static mechanical pressure-induced NPC apoptosis and IDD by activating the MAPK signaling pathway (mainly the p38 signaling pathway), inhibiting the ubiquitination of Nrf2 by Keap1 to promote Nrf2 phosphorylation and translocation to the nucleus and binding to ARE/EpRE. Ultimately, this induces the expression of antioxidant enzyme systems such as HO-1, inhibits intracellular ROS accumulation, improves NPC viability and inhibits apoptosis (Figure 9).

Our study also has some limitations that warrant attention. First, we did not examine the expression and protein conformational changes of Piezo1 under the influence of static mechanical stress, and we cannot definitively state that the accumulation of ROS in NPCs due to static mechanical stress results from the opening of Piezo1 ion channels through mechanical gating. Second, we did not test whether ADR affects the autophagic function of NPCs, which would impact the Nrf2 non-classical activation pathway. Third, we did not use PCR or immunofluorescence to further validate the reliability of the Western-blot results.

Abbreviations

IDD, intervertebral disc degeneration; LBP, low back pain; ADR, andrographolide; NPCs, nucleus pulposus cells; HE, Hematoxylin-eosin; ROS, reactive oxygen species; HO-1, heme oxygenase-1; IVD, intervertebral disk; NP, nucleus pulposus; ECM, extracellular matrix; ZnPP, Zinc protoporphyrin; Nrf2, NF-E2-related factor 2; MAPK, mitogen-activated protein kinase; TBHQ, tert-butylhydroquinone; RA, retinoic acid; SOD, superoxide dismutase; sMAF, mall Maf.

Acknowledgments

The authors thank Shulong Jiang and Luning Li (Clinical Medicine Laboratory Center, Jining No.1 People's Hospital, Jining Medical University, Jining, China) for their technical assistance. The manuscript was copy edited for English language by LetPub, with regard to grammar, punctuation, spelling, and clarity.

Author Contributions

All authors made a significant contribution to the work reported, whether that is in the conception, study design, execution, acquisition of data, analysis and interpretation, or in all these areas; took part in drafting, revising or critically reviewing the article; gave final approval of the version to be published; have agreed on the journal to which the article has been submitted; and agree to be accountable for all aspects of the work.

Funding

This research was funded by Jining City Key Research and Development Program Project, grant number 2020JKNS008, and Shandong Province Medical and Health Science and Technology Development Plan Project, grant number 202104070383.

Disclosure

The authors report no conflicts of interest in this work.

References

1. Ma K, Chen S, Li Z, et al. Mechanisms of endogenous repair failure during intervertebral disc degeneration. *Osteoarthritis Cartilage*. 2019;27(1):41–48.
2. Binch A, Fitzgerald JC, Growney EA, Barry F. Cell-based strategies for IVD repair: clinical progress and translational obstacles. *Nat Rev Rheumatol*. 2021;17(3):158–175.
3. Buchbinder R, van Tulder M, Oberg B, et al. Low back pain: a call for action. *Lancet*. 2018;391(10137):2384–2388.
4. Knezevic NN, Candido KD, Vlaeyen J, Van Zundert J, Cohen SP. Low back pain. *Lancet*. 2021;398(10294):78–92. doi:10.1016/S0140-6736(21)00733-9
5. Zhang HJ, Liao HY, Bai DY, Wang ZQ, Xie XW. MAPK /ERK signaling pathway: a potential target for the treatment of intervertebral disc degeneration. *Biomed Pharmacother*. 2021;143:112170. doi:10.1016/j.biopha.2021.112170
6. Bonnevie ED, Gullbrand SE, Ashinsky BG, et al. Aberrant mechanosensing in injured intervertebral discs as a result of boundary-constraint disruption and residual-strain loss. *Nat Biomed Eng*. 2019;3(12):998–1008. doi:10.1038/s41551-019-0458-4
7. Gullbrand SE, Ashinsky BG, Bonnevie ED, et al. Long-term mechanical function and integration of an implanted tissue-engineered intervertebral disc. *Sci Transl Med*. 2018;10:468. doi:10.1126/scitranslmed.aau0670
8. Schmidt H, Shirazi-Adl A. Temporal and spatial variations of pressure within intervertebral disc nuclei. *J Mech Behav Biomed Mater*. 2018;79:309–313. doi:10.1016/j.jmbbm.2018.01.012
9. Wang D, Chen Y, Cao S, et al. Cyclic mechanical stretch ameliorates the degeneration of nucleus pulposus cells through promoting the ITGA2/PI3K/AKT signaling pathway. *Oxid Med Cell Longev*. 2021;2021:6699326. doi:10.1155/2021/6699326
10. Fang H, Li X, Shen H, Sun B, Teng H, Li P. Osteogenic protein-1 attenuates apoptosis and enhances matrix synthesis of nucleus pulposus cells under high-magnitude compression though inhibiting the p38 MAPK pathway. *Biosci Rep*. 2018;38. doi:10.1042/BSR20180018
11. Tarabeih N, Kalinkovich A, Shalata A, Cherny SS, Livshits G. Deciphering the causal relationships between low back pain complications, metabolic factors, and comorbidities. *J Pain Res*. 2022;15:215–227.
12. Molladavoodi S, McMorran J, Gregory D. Mechanobiology of annulus fibrosus and nucleus pulposus cells in intervertebral discs. *Cell Tissue Res*. 2020;379(3):429–444.
13. Hancke JL, Srivastav S, Caceres DD, Burgos RA. A double-blind, randomized, placebo-controlled study to assess the efficacy of Andrographis paniculata standardized extract (ParActin(R)) on pain reduction in subjects with knee osteoarthritis. *Phytother Res*. 2019;33(5):1469–1479. doi:10.1002/ptr.6339
14. Cantelli M, Ferrillo M, Donnarumma M, Emanuele E, Fabbrocini G. A new proprietary gel containing glabridin, andrographolide, and apolactoferrin improves the appearance of epidermal melasma in adult women: a 6-month pilot, uncontrolled open-label study. *J Cosmet Dermatol*. 2020;19(6):1395–1398.
15. Phunikhom K, Khampitak K, Aromdee C, Arkaravichien T, Sattayasai J. Effect of andrographis paniculata extract on triglyceride levels of the patients with hypertriglyceridemia: a randomized controlled trial. *J Med Assoc Thai*. 2015;98(Suppl 6):S41–S47.
16. Wen T, Xu W, Liang L, et al. Clinical Efficacy of Andrographolide Sulfonate in the Treatment of Severe Hand, Foot, and Mouth Disease (HFMD) is Dependent upon Inhibition of Neutrophil Activation. *Phytother Res*. 2015;29(8):1161–1167. doi:10.1002/ptr.5361
17. Ciampi E, Uribe-San-Martin R, Carcamo C, et al. Efficacy of andrographolide in not active progressive multiple sclerosis: a prospective exploratory double-blind, parallel-group, randomized, placebo-controlled trial. *BMC Neurol*. 2020;20(1):173.
18. Juan CA, Perez DLLJ, Plou FJ, Perez-Lebena E. The Chemistry of Reactive Oxygen Species (ROS) revisited: outlining their role in biological macromolecules (DNA, Lipids and Proteins) and Induced Pathologies. *Int J Mol Sci*. 2021;22:9.
19. Solis AG, Bielecki P, Steach HR, et al. Mechanosensation of cyclical force by PIEZO1 is essential for innate immunity. *Nature*. 2019;573(7772):69–74. doi:10.1038/s41586-019-1485-8
20. Jiang F, Yin K, Wu K, et al. The mechanosensitive Piezo1 channel mediates heart mechano-chemo transduction. *Nat Commun*. 2021;12(1):869. doi:10.1038/s41467-021-21178-4
21. Wang B, Ke W, Wang K, et al. Mechanosensitive ion channel piezo1 activated by matrix stiffness regulates oxidative stress-induced senescence and apoptosis in human intervertebral disc degeneration. *Oxid Med Cell Longev*. 2021;2021:8884922.
22. Evans EL, Cuthbertson K, Endesh N, et al. Yoda1 analogue (Dooku1) which antagonizes Yoda1-evoked activation of Piezo1 and aortic relaxation. *Br J Pharmacol*. 2018;175(10):1744–1759. doi:10.1111/bph.14188
23. Dai Y, Chen SR, Chai L, Zhao J, Wang Y, Wang Y. Overview of pharmacological activities of Andrographis paniculata and its major compound andrographolide. *Crit Rev Food Sci Nutr*. 2019;59(sup1):S17–S29. doi:10.1080/10408398.2018.1501657
24. Ryter SW. Heme oxgenase-1, a cardinal modulator of regulated cell death and inflammation. *Cells-Basel*. 2021;10:3.
25. Morse D, Choi AM. Heme oxygenase-1: from bench to bedside. *Am J Respir Crit Care Med*. 2005;172(6):660–670. doi:10.1164/rccm.200404-465SO
26. Wu J, Li S, Li C, Cui L, Ma J, Hui Y. The non-canonical effects of heme oxygenase-1, a classical fighter against oxidative stress. *Redox Biol*. 2021;47:102170.
27. Li C, Stocker R. Heme oxygenase and iron: from bacteria to humans. *Redox Rep*. 2009;14(3):95–101. doi:10.1179/135100009X392584

28. Zhang CX, Wang T, Ma JF, Liu Y, Zhou ZG, Wang DC. Protective effect of CDDO-ethyl amide against high-glucose-induced oxidative injury via the Nrf2/HO-1 pathway. *Spine J*. 2017;17(7):1017–1025. doi:10.1016/j.spinee.2017.03.015
29. van der Pol A, van Gilst WH, Voors AA, van der Meer P. Treating oxidative stress in heart failure: past, present and future. *Eur J Heart Fail*. 2019;21(4):425–435. doi:10.1002/ejhf.1320
30. Kansanen E, Kuosmanen SM, Leinonen H, Levonen AL. The Keap1-Nrf2 pathway: mechanisms of activation and dysregulation in cancer. *Redox Biol*. 2013;1:45–49.
31. Itoh K, Wakabayashi N, Katoh Y, et al. Keap1 represses nuclear activation of antioxidant responsive elements by Nrf2 through binding to the amino-terminal Neh2 domain. *Genes Dev*. 1999;13(1):76–86. doi:10.1101/gad.13.1.76
32. Zhang Q, Zhang ZY, Du H, et al. DUB3 deubiquitinates and stabilizes NRF2 in chemotherapy resistance of colorectal cancer. *Cell Death Differ*. 2019;26(11):2300–2313. doi:10.1038/s41418-019-0303-z
33. Ugun-Klusek A, Tatham MH, Elkharaz J, et al. Continued 26S proteasome dysfunction in mouse brain cortical neurons impairs autophagy and the Keap1-Nrf2 oxidative defence pathway. *Cell Death Dis*. 2017;8(1):e2531. doi:10.1038/cddis.2016.443
34. Yamamoto M, Kensler TW, Motohashi H. The KEAP1-NRF2 system: a thiol-based sensor-effector apparatus for maintaining redox homeostasis. *Physiol Rev*. 2018;98(3):1169–1203. doi:10.1152/physrev.00023.2017
35. Tian H, Zhang B, Di J, et al. Keap1: one stone kills three birds Nrf2, IKKbeta and Bcl-2/Bcl-xL. *Cancer Lett*. 2012;325(1):26–34. doi:10.1016/j.canlet.2012.06.007
36. Pearson G, Robinson F, Beers GT, et al. Mitogen-activated protein (MAP) kinase pathways: regulation and physiological functions. *Endocr Rev*. 2001;22(2):153–183. doi:10.1210/edrv.22.2.0428
37. Park J, Kim YT. Erythronium japonicum alleviates inflammatory pain by inhibiting MAPK activation and by suppressing NF-kappaB activation via ERK/Nrf2/HO-1 signaling pathway. *Antioxidants*. 2020;9:7.
38. Han S, Gao H, Chen S, et al. Procyanidin A1 alleviates inflammatory response induced by LPS through NF-kappaB, MAPK, and Nrf2/HO-1 pathways in RAW264.7 cells. *Sci Rep*. 2019;9(1):15087. doi:10.1038/s41598-019-51614-x
39. Huang CY, Deng JS, Huang WC, Jiang WP, Huang GJ. Attenuation of lipopolysaccharide-induced acute lung injury by hispolon in mice, through regulating the TLR4/PI3K/Akt/mTOR and Keap1/Nrf2/HO-1 pathways, and suppressing oxidative stress-mediated ER stress-induced apoptosis and autophagy. *Nutrients*. 2020;12:6. doi:10.3390/nu12061742
40. Mildenberger J, Johansson I, Sergin I, et al. N-3 PUFAs induce inflammatory tolerance by formation of KEAP1-containing SQSTM1/p62-bodies and activation of NFE2L2. *Autophagy*. 2017;13(10):1664–1678. doi:10.1080/15548627.2017.1345411
41. Deng Z, Lim J, Wang Q, et al. ALS-FTLD-linked mutations of SQSTM1/p62 disrupt selective autophagy and NFE2L2/NRF2 anti-oxidative stress pathway. *Autophagy*. 2020;16(5):917–931. doi:10.1080/15548627.2019.1644076